

RESEARCH

Open Access



Prognostic and immunological implications of heterogeneous cell death patterns in prostate cancer

Ming Wang^{1†}, Bangshun Dai^{1†}, Qiushi Liu^{1†} and Xiansheng Zhang^{1*}

Abstract

Background Prostate cancer is one of the most common cancers in men with a significant proportion of patients developing biochemical recurrence (BCR) after treatment. Programmed cell death (PCD) mechanisms are known to play critical roles in tumor progression and can potentially serve as prognostic and therapeutic biomarkers in PCa. This study aimed to develop a prognostic signature for BCR in PCa using PCD-related genes.

Materials and methods We conducted an analysis of 19 different modes of PCD to develop a comprehensive model. Bulk transcriptomic, single-cell transcriptomic, genomic, and clinical data were collected from multiple cohorts, including TCGA-PRAD, GSE58812, METABRIC, GSE21653, and GSE193337. We analyzed the expression and mutations of the 19 PCD modes and constructed, evaluated, and validated the model.

Results Ten PCD modes were found to be associated with BCR in PCa, with specific PCD patterns exhibited by various cell components within the tumor microenvironment. Through Lasso Cox regression analysis, we established a Programmed Cell Death Index (PCDI) utilizing an 11-gene signature. High PCDI values were validated in five independent datasets and were found to be associated with an increased risk of BCR in PCa patients. Notably, older age and advanced T and N staging were associated with higher PCDI values. By combining PCDI with T staging, we constructed a nomogram with enhanced predictive performance. Additionally, high PCDI values were significantly correlated with decreased drug sensitivity, including drugs such as Docetaxel and Methotrexate. Patients with lower PCDI values demonstrated higher immunophenoscores (IPS), suggesting a potentially higher response rate to immune therapy. Furthermore, PCDI was associated with immune checkpoint genes and key components of the tumor microenvironment, including macrophages, T cells, and NK cells. Finally, clinical specimens validated the differential expression of PCDI-related PCDRGs at both the gene and protein levels.

Conclusion In conclusion, we developed a novel PCD-based prognostic feature that successfully predicted BCR in PCa patients and provided insights into drug sensitivity and potential response to immune therapy. These findings have significant clinical implications for the treatment of PCa.

[†]Ming Wang, Bangshun Dai and Qiushi Liu contributed equally to this work.

*Correspondence:
Xiansheng Zhang
xiansheng-zhang@163.com

Full list of author information is available at the end of the article



© The Author(s) 2024. **Open Access** This article is licensed under a Creative Commons Attribution-NonCommercial-NoDerivatives 4.0 International License, which permits any non-commercial use, sharing, distribution and reproduction in any medium or format, as long as you give appropriate credit to the original author(s) and the source, provide a link to the Creative Commons licence, and indicate if you modified the licensed material. You do not have permission under this licence to share adapted material derived from this article or parts of it. The images or other third party material in this article are included in the article's Creative Commons licence, unless indicated otherwise in a credit line to the material. If material is not included in the article's Creative Commons licence and your intended use is not permitted by statutory regulation or exceeds the permitted use, you will need to obtain permission directly from the copyright holder. To view a copy of this licence, visit <http://creativecommons.org/licenses/by-nc-nd/4.0/>.

Keywords Prostate cancer, Biochemical recurrence, Programmed cell death, Tumor microenvironment, Drug sensitivity, Immune therapy

Introduction

Prostate cancer (PCa) is a prevalent malignancy affecting the urogenital system and ranks as the second leading cause of cancer-related mortality among men [1]. The incidence of prostate cancer notably rises with advancing age, particularly in males aged 50 years and older [2, 3]. While early-stage prostate cancer patients generally exhibit a favorable prognosis with low mortality rates, those with distant metastasis face an overall survival rate of less than 30% [4]. Furthermore, a considerable proportion of PCa patients ultimately develop resistance to androgen deprivation therapy, leading to the emergence of castration-resistant prostate cancer and a shortened survival time [5]. Approximately one-third of prostate cancer patients experience biochemical recurrence (BCR) following local treatment [6], which presents a significant concern for individuals who have undergone initial curative interventions. Timely detection of recurrent disease plays a crucial role in facilitating salvage treatment with curative intent. Therefore, identifying robust prognostic biomarkers and deciphering the molecular pathways underlying BCR are imperative for refining risk categorization and customizing therapy in PCa.

Programmed Cell Death (PCD) represents a fundamental cellular regulatory mechanism that maintains the proper development and functionality of tissues and organs in a controlled manner. However, in the context of cancer, the dysregulation of PCD processes frequently occurs, resulting in the uncontrolled proliferation and survival of aberrant cells. Remarkably, PCD encompasses a diverse array of molecular pathways, encompassing 19 distinct mechanisms including Apoptosis, Pyroptosis, Ferroptosis, Autophagy, Necroptosis, Cuproptosis, Parthanatos, Entotic cell death, Netotic cell death, Lysosome-dependent cell death, Alkaliptosis, Oxeiptosis, NETosis, Immunogenic cell death, Anoikis, Paraptosis, Methuosis, Entosis, and Disulfidptosis [7, 8]. Apoptosis, extensively investigated as the central form of PCD, plays a fundamental role in maintaining tissue homeostasis by eliminating senescent or unnecessary cells [9]. Pyroptosis, triggered by inflammasome activation and caspase-1 cleavage, represents an inflammatory form of PCD [10]. Ferroptosis, dependent on intracellular iron accumulation, lipid peroxidation, and membrane rupture, constitutes an oxidative cell death process [11]. Autophagy, a self-regulatory mechanism, facilitates the degradation and recycling of cellular components through lysosomes [12]. Necroptosis, mediated by the activation and interaction of critical genes such as RIPK1, RIPK3, and MLKL, closely intertwines with inflammatory responses

and immune regulation [13]. Cuproptosis, initiated by copper overload and activated by lipid peroxidation and mitochondrial dysfunction, represents a specific PCD pathway [14]. Parthanatos, induced by DNA damage, manifests through DNA fragmentation, PARP-1 activation, PAR accumulation, and mitochondrial dysfunction [15]. Entotic cell death, involving cellular engulfment, actively participates in cell adhesion, intracellular signaling, and cytoskeletal remodeling [16]. Netotic cell death is distinguished by the formation and release of extracellular traps (NETs) and is regulated by NET formation-related proteins (such as PAD4) and cell death signaling pathways (such as RIPK1) [17]. Lysosome-dependent cell death arises from the disruption of lysosomal function, leading to the release of its contents [18]. Alkaliptosis, provoked by alkaline conditions, is characterized by elevated intracellular pH, resulting in mitochondrial dysfunction, increased ROS generation, and cell membrane rupture [19]. Oxeiptosis, an apoptotic-like cell death pathway, is induced by reactive oxygen species (ROS) independently of caspase activation [20]. NETosis involves chromatin decondensation and nuclease release mediated by PAD4, leading to the release of DNA webs (NETs) by neutrophils to immobilize and eliminate pathogens [21]. Immunogenic cell death triggers an immune response by activating intracellular signaling pathways such as endoplasmic reticulum stress, mitochondrial dysfunction, and release of intracellular proteins, ultimately stimulating immune cell activation and anti-tumor immune responses [22]. Anoikis, initiated by the loss of appropriate attachment to the extracellular matrix, represents a specific form of PCD [23]. Paraptosis, distinguished by cell swelling, mitochondrial enlargement, and endoplasmic reticulum breakdown, constitutes a non-apoptotic form of cell death [24]. Methuosis involves lysosomal enlargement, cytoplasmic dissolution, and subsequent cell breakdown and death [25]. Entosis involves cell internalization and death through cell engulfment [26]. Finally, Disulfidptosis, recently unveiled as a cell death mechanism, promotes cell demise through the generation and disruption of intracellular disulfide bonds, involving oxidative stress, cell membrane rupture, and the release of cellular contents [27].

In recent years, there has been a growing recognition of the significant role that PCD plays in the development and progression of malignant tumors. By leveraging the existing knowledge of PCD-related genes (PCDRGs), it is possible to construct risk models that can offer valuable prognostic assessments and customized treatment

guidance for patients with malignant tumors. However, a comprehensive synthesis of the relationship between PCDRGs and cancer in PCa is currently lacking, and there exists a dearth of research concerning the intricate functional mechanisms of PCD in PCa. Therefore, the primary objective of this study is to establish a novel parameter, termed the Programmed Cell Death Index (PCDI), with the purpose of evaluating BCR and treatment response among PCa patients. In summary, our investigation demonstrated the existence of heterogeneity among prostate cancer patients, enabling the assessment of their clinical prognosis. Furthermore, this study has the potential to contribute to the identification of appropriate treatment strategies for individuals afflicted

with prostate cancer. Figure 1 provides a visual representation of the study's methodology.

Materials and methods

Data acquisition and preprocessing

The set of PCD-related genes encompasses critical regulatory genes within the aforementioned 19 PCD pathways. These genes were curated from various authoritative sources, including GSEA gene sets, KEGG databases, review articles, and meticulous manual curation [28]. The final compilation comprises 19 categories of genes associated with PCD, comprising 580 genes related to apoptosis, 52 genes related to pyroptosis, 88 genes related to ferroptosis, 367 genes related to autophagy, 101 genes related to necroptosis, 19 genes related

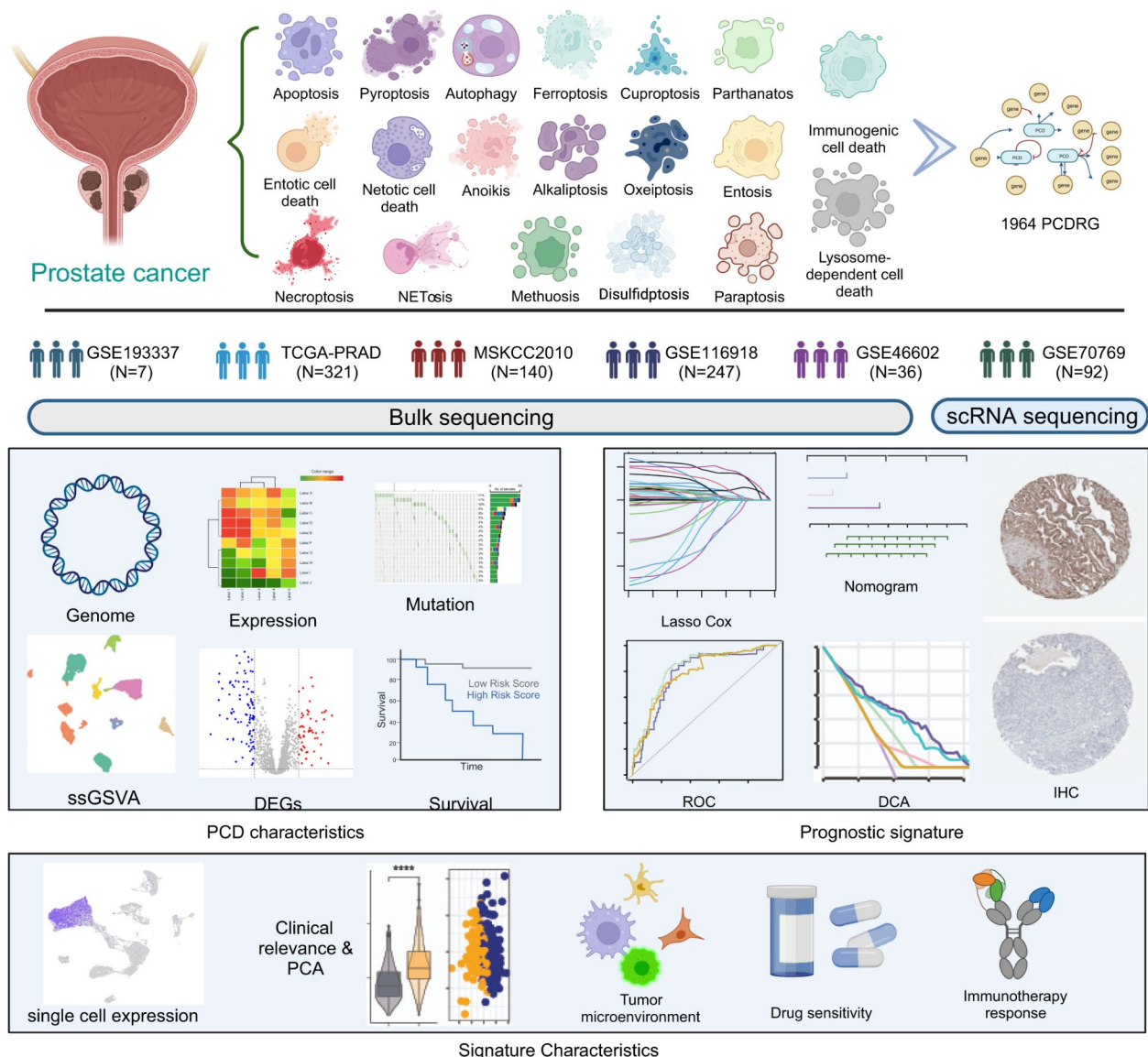


Fig. 1 Flowchart for comprehensive analysis of diverse cell death patterns in patients with prostate cancer (PCa)

to cuproptosis, 9 genes related to parthanatos, 15 genes related to entotic cell death, 8 genes related to netotic cell death, 220 genes related to lysosome-dependent cell death, 7 genes related to alkaliptosis, 5 genes related to oxeiptosis, 24 genes related to NETosis, 34 genes related to immunogenic cell death, 338 genes related to anoikis, 66 genes related to paraptosis, 9 genes related to methuosis, 24 genes related to entosis, and 16 genes related to disulfidptosis [29]. Altogether, the analysis incorporated a total of 1964 concatenated genes associated with PCD (Supplementary materials: Table S1).

We retrieved transcriptomic, mutation, and clinical data of TCGA-PRAD from The Cancer Genome Atlas (TCGA, <https://portal.gdc.cancer.gov>). Additionally, we obtained 247 samples from the GSE116918 dataset, 36 samples from the GSE46602 dataset, 92 samples from the GSE70769 dataset, and single-cell transcriptomic data from the GSE193337 dataset, which encompasses single-cell sequencing data from 4 PCa and 4 benign tissues. Furthermore, we acquired data from MSKCC2010, comprising 140 samples, from cBioPortal (<https://www.cbioportal.org/>). All datasets underwent normalization utilizing the Fragments Per Kilobase of transcript per Million mapped reads (FPKM) methodology [30], followed by log₂ transformation to stabilize variance and enhance data symmetry. The R package “sva” was applied to mitigate batch effects [31]. Following the exclusion of duplicates and cases with incomplete prognostic information, a total of 321 cases from the TCGA-PRAD cohort were included in the construction of our model.

Differential expression and mutation of PCDRG

Raw transcriptomic count data for a total of 497 PCa patients and 51 normal tissues from the TCGA-PRAD cohort were subjected to preparation. Differential expression analysis of PCD-related genes (dePCDRGs) was conducted using the “limma” package, applying a screening criterion of statistical significance ($P < 0.05$) and fold change threshold ($|\log_2FC| > 1$). To investigate and visualize the somatic mutation landscape within PCa patients, we employed the “maftools” package [32]. Furthermore, for the purpose of elucidating the chromosomal location, gene expression patterns, and co-expression correlations pertaining to dePCDRGs, we utilized the “RCircos” R package [33].

Functional enrichment analysis

We conducted gene ontology (GO) and Kyoto Encyclopedia of Genes and Genomes (KEGG) analyses on the dePCDRGs using the “clusterProfiler” R package [34]. In brief, we initially converted the gene symbols of the dePCDRGs to Entrez IDs and performed a barplot visualization, applying a significance threshold of $p < 0.05$.

Construction of PCD prognostic model

Initially, we employed univariate Cox regression to evaluate the impact of dePCDRGs on BCR in patients with PCa. Subsequently, dePCDRGs significantly associated with BCR at a significance level of $p < 0.01$ were identified. To further refine the candidate signature, we utilized the LASSO Cox regression method with the glmnet package, employing the deviance method for loss in cross-validation. This enabled us to construct the most appropriate signature for our analysis. The resulting model generated a PCDI for each patient, which was calculated as follows: $PCDI = \sum \beta_i * Exp_i$, where β_i represents the risk coefficient for each gene and Exp_i denotes the expression level of each gene. We divided all patient cohorts into two groups, namely High_PCDI and Low_PCDI, based on the median value of PCDI. To assess the survival outcomes of these groups, Kaplan-Meier analysis was performed using the “survival” and “survminer” packages. To evaluate the discriminative ability of PCDI-related genes, we employed principal component analysis. The prognostic performance of the model was assessed using the receiver operating characteristic (ROC) curve. Additionally, we validated the protein expression levels of PCDI-related genes using the Human Protein Atlas (HPA) database (<https://www.proteinatlas.org/>).

Construction of nomogram

Univariate and multivariate Cox regression analyses were employed to evaluate the prognostic significance and relevance of clinical features, namely age, T stage, N stage, and the PCDI. A prognostic nomogram was constructed utilizing the “rms” package, and the resulting nomogram was visualized using the “regplot” package. To assess the calibration and predictive accuracy of the nomogram, calibration plots, decision curve analysis (DCA), and ROC analysis were utilized. These rigorous evaluations were conducted to determine the prognostic performance and clinical utility of the constructed nomogram.

Tumor microenvironment analysis

The CIBERSORT method, a robust computational algorithm, was utilized to assess the proportions of 22 distinct tumor-infiltrating immune cell (TIIC) subsets [35]. The Wilcoxon test was employed to compare the variations in immune infiltration levels between the High_PCDI group and the Low_PCDI group. Furthermore, the correlation between PCDI and immunomodulators was analyzed.

Treatment response analysis

The sensitivity analysis of 43 drugs were conducted using the pRRophetic package [36], and the correlation between PCDI and its associated genes with drug sensitivity were analyzed. The tumor immune dysfunction

and exclusion (TIDE) algorithm (<http://tide.dfci.harvard.edu/>) was utilized to calculate the TIDE score. The Cancer Immunome Atlas (TCIA) database (<https://tcia.at/>) was employed to acquire the immunophenoscores (IPS) of PCa [37], which enabled the prediction of patients' response to immune checkpoint blockade (ICB) therapy targeting PD-L1, PD-1, and CTLA4 [38].

scRNA-Seq data processing

Following established protocols [39], the single-cell transcriptome data analysis and visualization were conducted utilizing the "Seurat" package. Initially, a Seurat object was created to facilitate the integration of 8 single-cell sequencing samples. Cells with fewer than 201 or more than 8,000 expressed genes were excluded, as well as those with mitochondrial gene expression exceeding 20%. The FindVariableFeatures function was utilized to identify the top 3000 highly variable genes. Principal component analysis (PCA) was subsequently performed using these 3000 genes, followed by dimensionality reduction and cluster identification using uniform manifold approximation and projection (UMAP). Cell annotation was conducted based on well-established marker genes from published literature. To further investigate gene set variation at the single-cell level, the GSVA package was employed.

Sample collection

PCa specimens and corresponding adjacent tissues were procured from five patients. These samples were swiftly preserved by immersion in liquid nitrogen and stored at -80°C for future analysis. Comprehensive informed consent was obtained from all participants and their families prior to sample collection. The Ethics Committee of the Department of Urology at the First Affiliated Hospital of Anhui Medical University granted approval for this study.

Quantitative real-time polymerase chain reaction (qRT-PCR)

RNA was extracted using TRIzol reagent (Thermo Scientific, USA) following the manufacturer's protocol. A total of 2 μg RNA was used to synthesize cDNA using the RevertAid First Strand cDNA Synthesis Kit (Thermo Scientific, USA). qRT-PCR was performed using SYBR Green Mix (Vazyme, Nanjing, China) to detect the expression of target genes. Quantitative data were normalized by GAPDH. The primer sequences involved in the experiments were listed in Supplementary materials: Table S2.

Western blot

Tissues were lysed with RIPA buffer. 25 μg of protein quantified by a BCA kit were subjected to 10% SDS-PAGE and transferred to a polyvinylidene fluoride

membrane. The membrane was blocked with 5% non-fat milk and incubated overnight at 4°C with primary antibodies against GAPDH, NOX4, AFP, and ATP6V0D2 (Abcam, Cambridge, UK). Goat anti-mouse and anti-rabbit antibodies conjugated with horseradish peroxidase served as secondary antibodies (Abcam, Cambridge, UK), and the blots were detected using enhanced chemiluminescence (ECL) (Dura, Pierce, NJ, USA).

Statistical analyses

All statistical analyses were performed using R software version 4.2.2. The comparison of differences between two groups was conducted using either the Student's t-test or the Wilcoxon test. Statistical significance was established at a p-value threshold of less than 0.05.

Results

Differential expression and mutations of PCDRGs

In the TCGA-PRAD cohort, a total of 146 dePCDRGs were identified, meeting the criteria of $P < 0.05$ and $|\log_2\text{FC}| > 1$. Of these, 56 genes exhibited upregulation, while 90 genes displayed downregulation specifically in prostate cancer. The full list of these genes can be found in Supplementary materials: Table S3. To visually represent the gene expression patterns, a heatmap of the scaled dePCDRGs levels (Fig. 2A) and a volcano plot illustrating the dePCDRGs (Fig. 2B) were generated. Additionally, Fig. 2C provides detailed information on the chromosomal positions, expression levels, and correlations of each dePCDRGs. Subsequent enrichment analyses revealed that these dePCDRGs are involved in diverse biological pathways. Notably, the pathways implicated include PI3K-AKT, Ras and Rap1 signaling pathways, as well as necroptosis, apoptosis, and autophagy pathways and processes (Fig. 2D and E). In the TCGA-PRAD dataset, 60.81% of prostate cancer patients exhibited mutations. A comprehensive analysis of the top 20 most frequently mutated genes among the dePCDRGs was visualized in the oncoplot, with SPOP (11%), TP53 (11%), and TTN (10%) displaying the highest mutation frequencies (Fig. 2F). Moreover, analysis of copy number variations (CNVs) in the dePCDRGs revealed widespread alterations. Notably, TNFRSF10C, ADRA1A, and CLU exhibited significant copy number loss, while TP53INP1, ATP6V0D2, and CHMP4C showed substantial copy number amplification (Fig. 2G).

Prognostic-related PCD and PCDRGs

Cox regression analysis was performed to evaluate the association between dePCDRGs and BCR in PCa. The analysis identified a total of 41 dePCDRGs that showed significant correlation with BCR in PCa ($p < 0.05$, Supplementary materials: Table S4). Figure 3A illustrates the gene expression, hazard ratio, and corresponding PCD

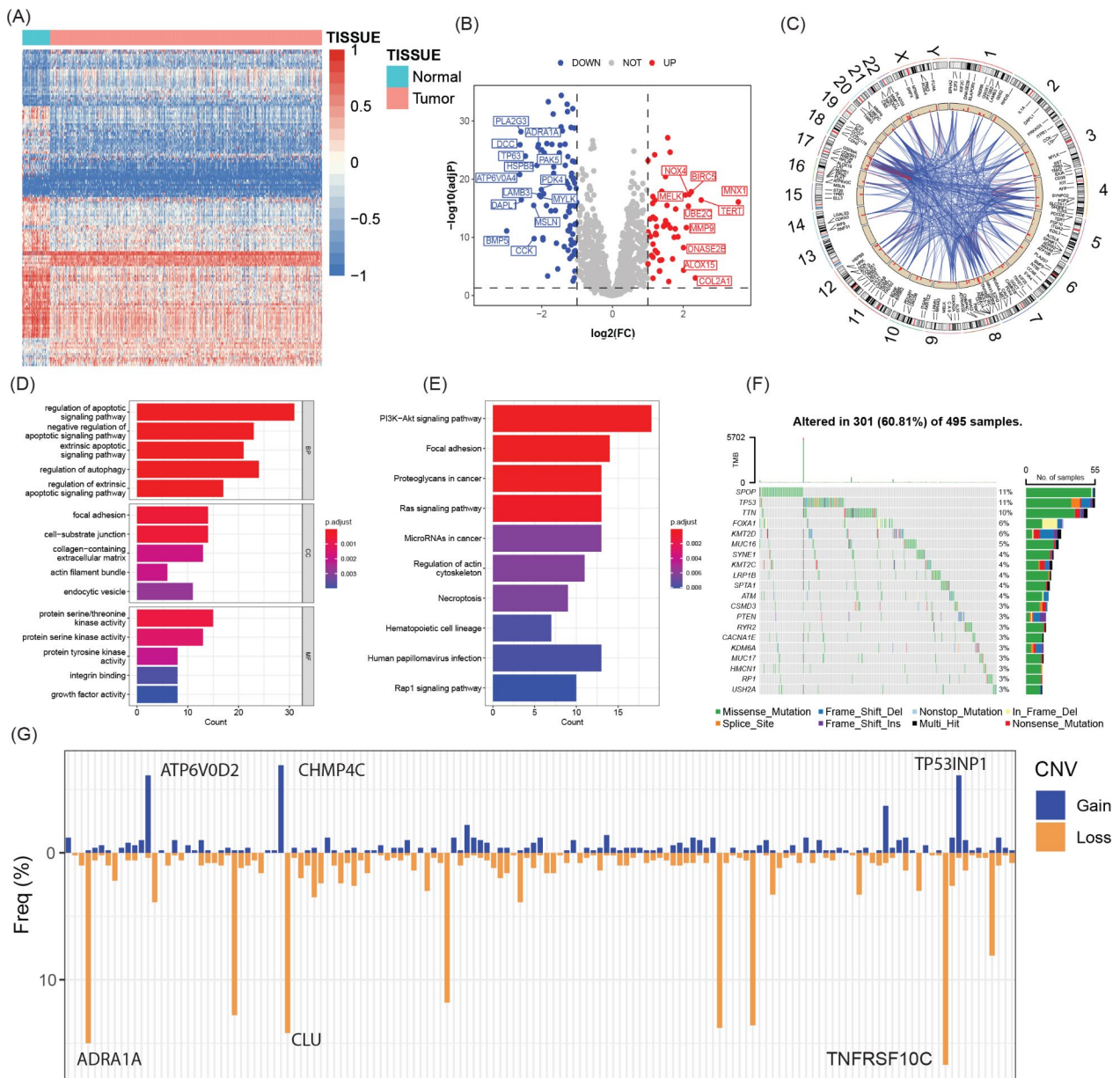


Fig. 2 Variant landscape of programmed cell death genes in prostate cancer patients in the TCGA-PRAD cohort. **(A)** Heatmap illustrating the differential expression of dePCDRGs between prostate cancer tissues and normal tissues. **(B)** Volcano plot highlighting the dePCDRGs with statistical significance. Thresholds include a P-value < 0.01 and $|\log_2\text{FC}| > 1$. **(C)** Visualization of the location, expression, and correlation of dePCDRGs. **(D)** Gene Ontology (GO) enrichment analysis of the dePCDRGs. **(E)** Kyoto Encyclopedia of Genes and Genomes (KEGG) enrichment analysis of the dePCDRGs. **(F)** OncoPrint displaying the top 20 dePCDRGs with more frequent mutations. **(G)** Barplot indicating the frequency of copy number variations (CNV) in dePCDRGs

patterns of these BCR-associated PCDRGs. The results revealed the presence of 10 distinct PCD patterns, shedding light on potential mechanisms underlying BCR in PCa patient. Further analysis using single-cell transcriptome analysis and annotation enabled the identification of 7 major cell clusters, which included endothelial cells, T cells, B cells, macrophages & monocytes, fibroblasts, epithelial cells, and mast cells (Fig. 3B). To assess the enrichment status of the 10 prognostic-related PCD patterns, ssGSVA analysis was performed (Fig. 3C). The

analysis revealed that entosis, NETosis, paraptosis, and necroptosis exhibited lower enrichment scores in cancer tissues, while ferroptosis displayed higher enrichment scores. Moreover, other PCD patterns demonstrated certain heterogeneity across different cell types.

Construction of PCDI and its clinical relevance

To further investigate the prognostic potential of the identified dePCDRGs, a lasso Cox regression analysis was performed in addition to the Cox regression analysis.

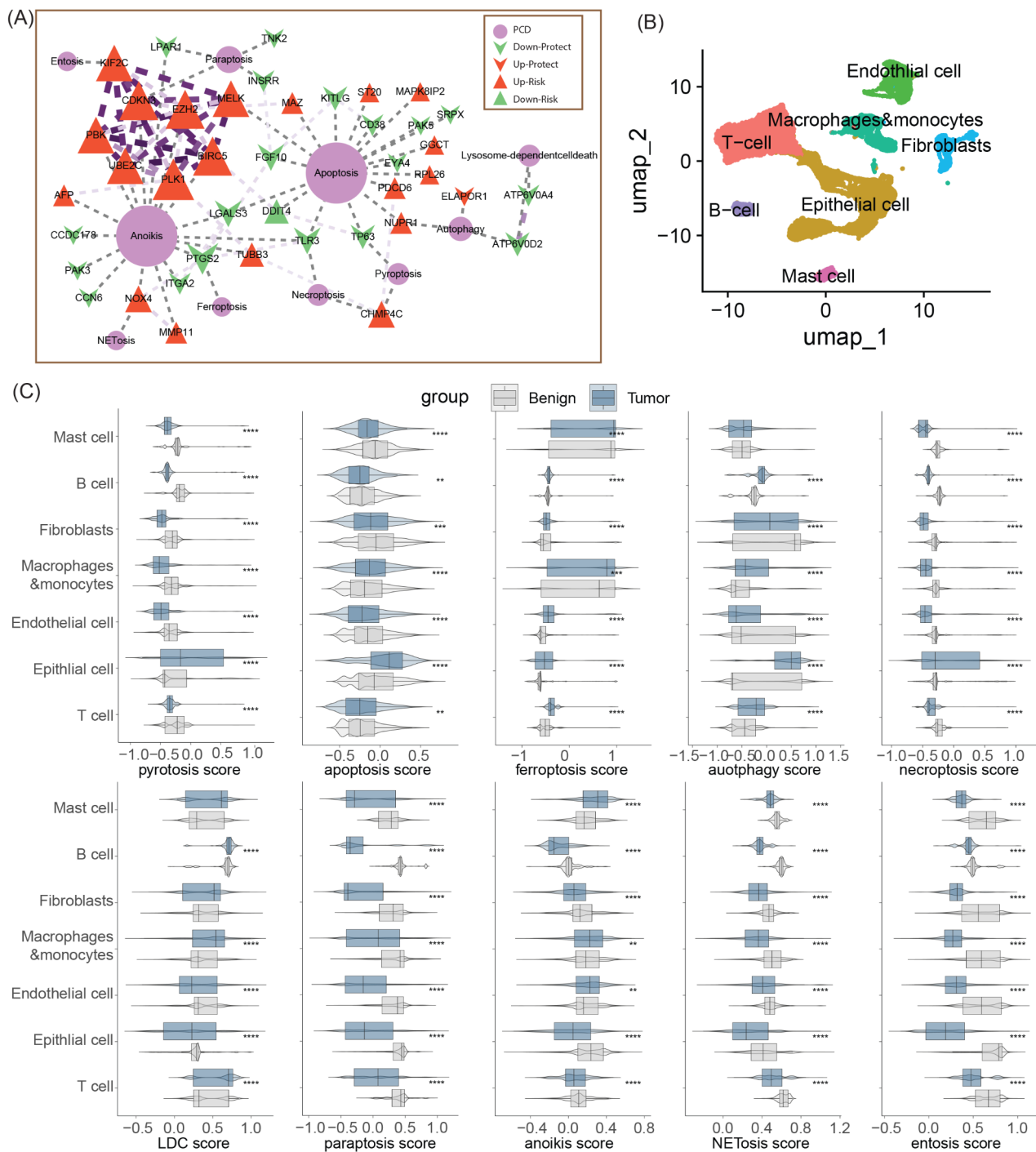


Fig. 3 Landscape of PCDRGs associated with BCR in PCa patients. **(A)** Network illustrating the relationship between prognosis-related PCDs and differentially expressed PCD-related genes. **(B)** Cell cluster annotation based on data from the GSE19337 cohort. **(C)** Comparison of the single-sample gene set variation analysis (ssGSVA) score of prognosis-related PCDs across different cell clusters. Statistical significance: ** $p < 0.01$, *** $p < 0.001$, **** $p < 0.0001$

This analysis resulted in the selection of 11 genes that were highly associated with BCR in PCa patients, forming the basis of a prognostic model (Fig. 4A and B, Figure S1). The coefficients of these 11 genes are presented in Fig. 4C, highlighting the protective effect of INSRR and

ATP6V0D2 against BCR in PCa patients, while the other 9 genes act as risk factors. Specifically, the signature was calculated using the following formula: $PCDI = 0.06 * TNK2 + 0.915 * ST20 + 0.288 * NOX4 + 0.313 * MMP11 + 0.137 * MAZ - 0.515 * INSRR + 0.216 *$

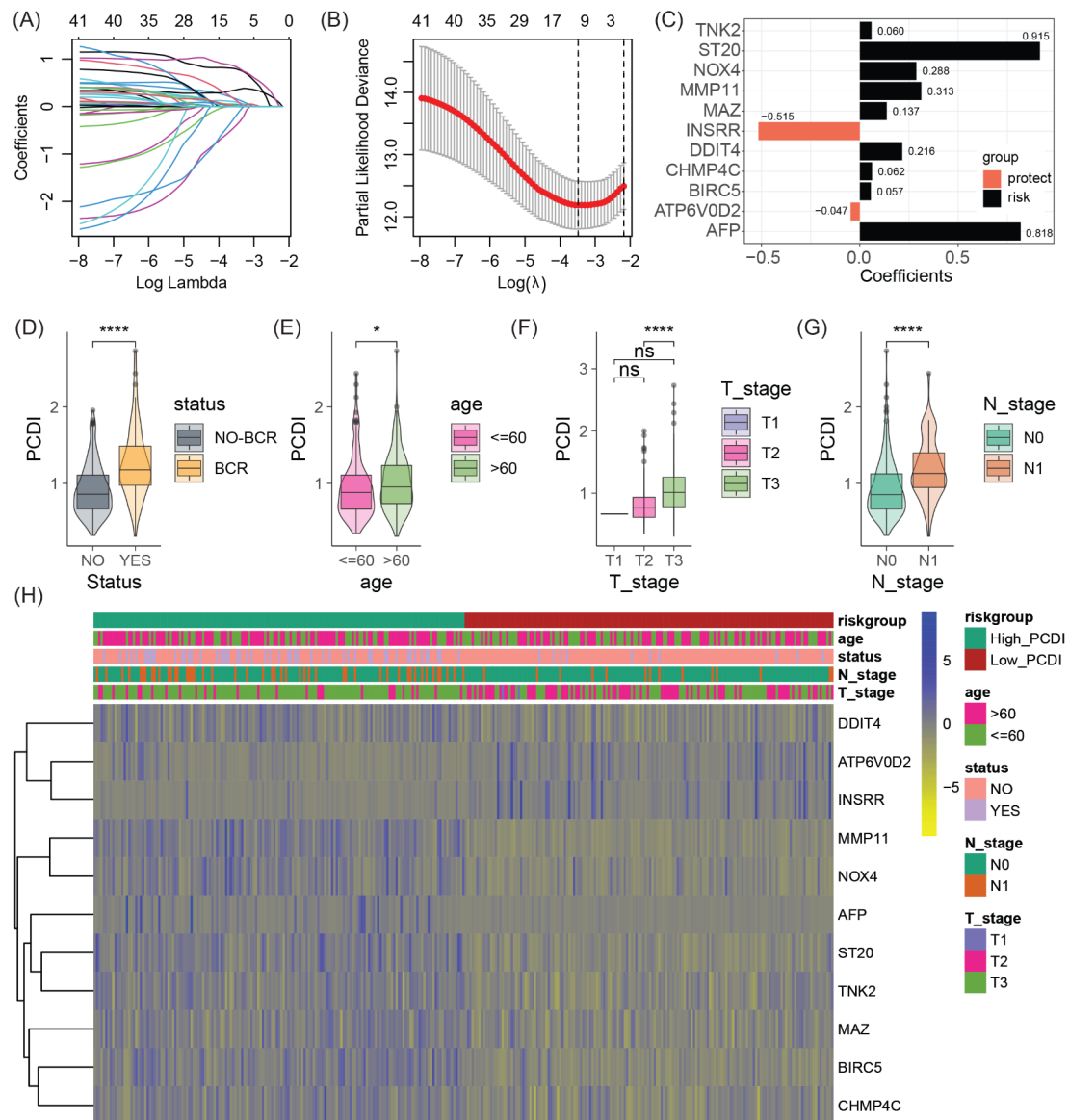


Fig. 4 Development of a prognostic signature for PCa patients based on prognosis-related dePCDRGs. **(A)** Identification of the 11 PCDRGs using lasso Cox regression analysis. **(B)** Cross-validation of the constructed signature. **(C)** Coefficients of the 11 PCDRGs in the risk signature. Comparison of the programmed cell death index (PCDI) among different subgroups stratified by status **(D)**, age **(E)**, T_{stage} **(F)**, and N_{stage} **(G)**. **(H)** Heatmap displaying the expression levels of the 11 PCDs in the signature and their association with clinicopathological characteristics. Statistical significance: **p* < 0.05, *****p* < 0.0001

DDIT4+0.062 * CHMP4C+0.057 * BIRC5−0.047 * ATP6V0D2+0.818 * AFP. Based on the median PCDI value, the 321 PCa patients in the TCGA cohort were divided into High_PCDI and Low_PCDI groups, which were then used as the training dataset. PCDI displayed significant associations with various clinical features of PCa, including different survival statuses (BCR and non-BCR), T stages (T1-T3), and N stages (N0-N1) (Fig. 4D-H).

Validation of PCDI features

Subsequently, PCDI values were calculated for all cohorts, and based on the median value, the cohorts were divided into two groups: High_PCDI and Low_PCDI (Fig. 5A). Scatter plots of BCR time for these cohorts are presented in Fig. 5B. Principal component analysis (PCA) was performed to assess the classification effectiveness of PCDI-related genes in the TCGA-PRAD, MSKCC2010, GSE46602, and GSE70769 cohorts, while the GSE116918 cohort exhibited suboptimal performance (Fig. 5C). Furthermore, Kaplan-Meier analysis revealed a significantly higher probability of BCR in the

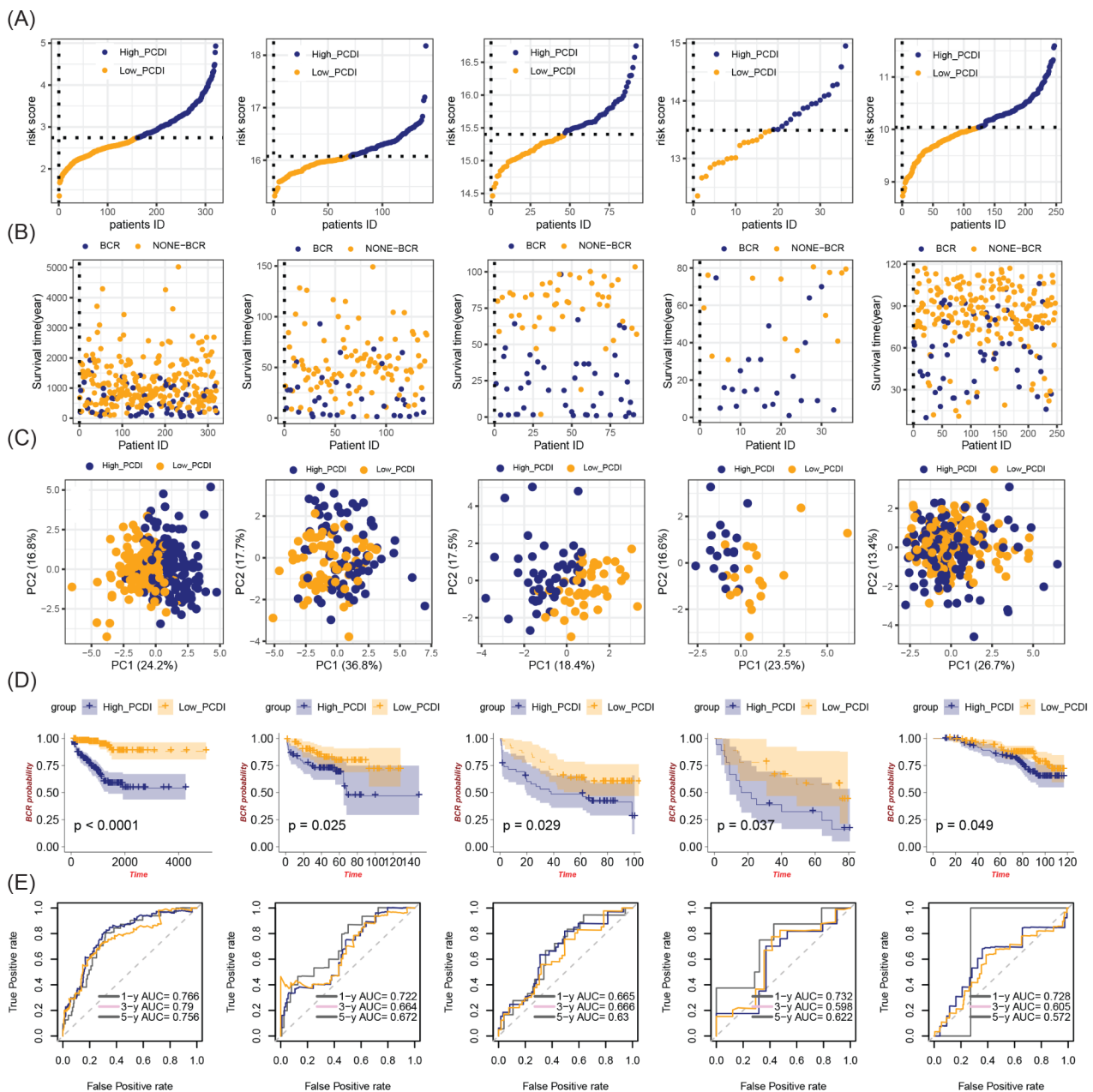


Fig. 5 Internal training and external validation of the PCDI signature. **(A)** Distribution of adjusted PCDI values based on survival status **(A)** and time **(B)** in the TCGA, MSKCC2010, GSE116918, GSE46602, GSE70769 cohorts. **(B)** Principal component analysis (PCA) plot illustrating the clustering of samples based on the PCDI-related PCDRGs in the TCGA, MSKCC2010, GSE116918, GSE46602, GSE70769 cohorts. **(C–D)** Analysis of overall survival, disease-free survival, and recurrence-free survival between low-PCDI and high-PCDI group patients in the TCGA, MSKCC2010, GSE116918, GSE46602, GSE70769 cohorts. **(E)** The prognostic performance of the PCDI model was evaluated through ROC analysis

High_PCDI group compared to the Low_PCDI group in TCGA-PRAD ($p < 0.001$), MSKCC2010 ($p = 0.025$), GSE70769 ($p = 0.029$), GSE46602 ($p = 0.037$), and GSE116918 ($p = 0.049$) (Fig. 5D). ROC analysis revealed that in the TCGA-PRAD cohort (Fig. 5E), the area under the curve (AUC) for PCDI-based prediction of BCR at 1, 3, and 5 years was 0.766, 0.790, and 0.756, respectively. In the MSKCC2010 cohort, the corresponding AUC

values were 0.722, 0.664, and 0.672. For the GSE70769 cohort, the AUCs were 0.665, 0.666, and 0.630 at these time points. In the GSE46602 cohort, the AUCs were 0.732, 0.598, and 0.622, while in another analysis of the GSE70769 cohort, they were 0.728, 0.605, and 0.572, respectively.

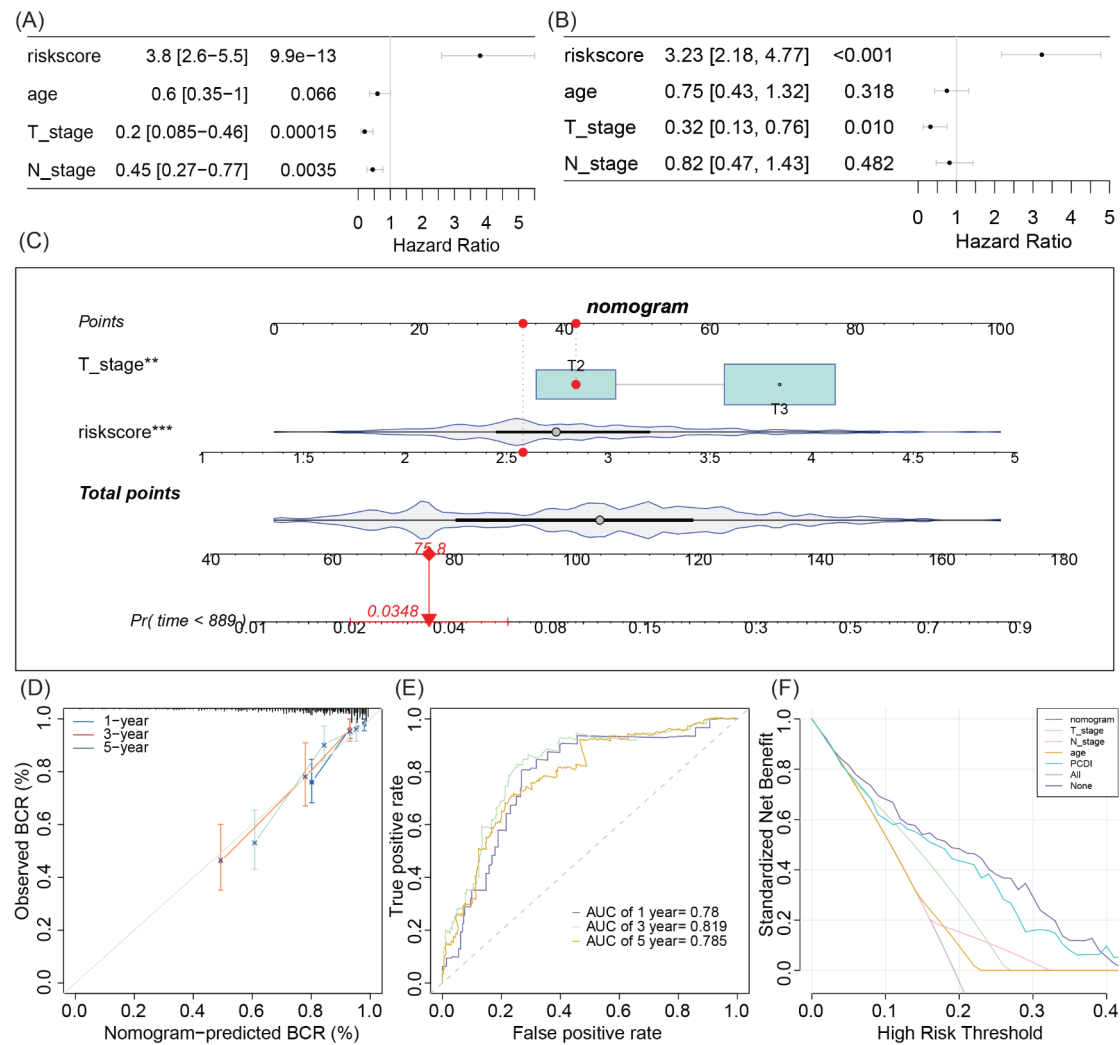


Fig. 6 Establishment and evaluation of the nomogram-based survival model using the TCGA-PRAD cohort. **(A)** Univariate analysis of clinicopathological characteristics and programmed cell death index (PCDI). **(B)** Multivariate analysis of clinicopathological characteristics and PCDI. **(C)** Development of a nomogram for predicting the prognosis of prostate cancer (PCa) patients. **(D)** Calibration plots demonstrating the probability of 1-, 3-, and 5-year biochemical recurrence (BCR). **(E)** Receiver operating characteristic (ROC) analysis of the nomogram in the TCGA cohort. **(F)** Decision curve analysis (DCA) of the nomogram for predicting 1-year BCR probability

Predicting BCR in PCa patients through PCDI combined with T stage

Univariate and multivariate Cox regression analyses were employed to assess the potential independent prognostic value of PCDI. The results of the univariate Cox regression analysis indicated that PCDI exhibited a significantly higher risk compared to other variables (HR=3.8, 95% CI: 2.6~5.5, $P<9.9e-13$, Fig. 6A). Furthermore, upon adjusting for confounding factors, the multivariate analysis confirmed PCDI as an independent prognostic factor in patients with PCa (HR=3.23, 95% CI: 2.18~4.77, $P<0.001$, Fig. 6B). To enable the estimation of 1-year, 3-year, and 5-year BCR, a nomogram model was developed using multivariable Cox and stepwise regression analyses based on data from the TCGA cohort. This model incorporated PCDI and T stage as predictive

factors (Fig. 6C). The calculated c-index of the model was 0.7752, indicating good discriminative ability. Calibration curves were plotted to assess the accuracy of the model in predicting 1-year, 3-year, and 5-year survival rates (Fig. 6D). Additionally, ROC analysis demonstrated the high predictive accuracy of the nomogram for 1, 3, and 5-year BCR in the TCGA-PRAD queue, with corresponding area under the curve (AUC) values of 0.78, 0.819, and 0.785, respectively (Fig. 6E). Furthermore, decision curve analysis (DCA) illustrated the superiority of the nomogram model over other predictors utilized in this study (Fig. 6F).

PCDI features indicate drug sensitivity and immune therapy response

To investigate the association between the model and drug sensitivity, we performed a comprehensive analysis of the TCGA-PRAD cohort in relation to 43 drugs, taking into account their correlation with PCDI and its associated genes. The correlation and statistical significance of drug sensitivity with PCDI are depicted in Fig. 7A, revealing a predominantly negative correlation between PCDI and drug sensitivity. Specifically, our analysis revealed that patients in the High_PCDI group exhibited lower sensitivity to Docetaxel and Methotrexate, while showing higher sensitivity to Cisplatin (Fig. 7B-G). These findings suggest that PCa patients with elevated PCDI levels may demonstrate resistance to conventional chemotherapy regimens, yet exhibit enhanced sensitivity to Cisplatin. Furthermore, we assessed the TIDE scores

in each PCa patient, but no significant differences were observed (Fig. 7H). Lastly, we evaluated the therapeutic efficacy of immune checkpoint inhibitors by employing IPS. The results demonstrated that among patients receiving CTLA4 and PD1 blockade therapy, the IPS of the High_PCDI group was significantly lower compared to the Low_PCDI group (Fig. 7I). Collectively, these findings highlight the potential of PCDI as a valuable prognostic indicator for guiding drug selection and immune-based therapies.

PCDI is associated with the tumor microenvironment

The correlation analysis conducted in this study revealed a statistically significant relationship between PCDI and a range of immune modulators, predominantly characterized by negative correlations (Fig. 8A). These findings suggest that patients with lower PCDI levels may exhibit

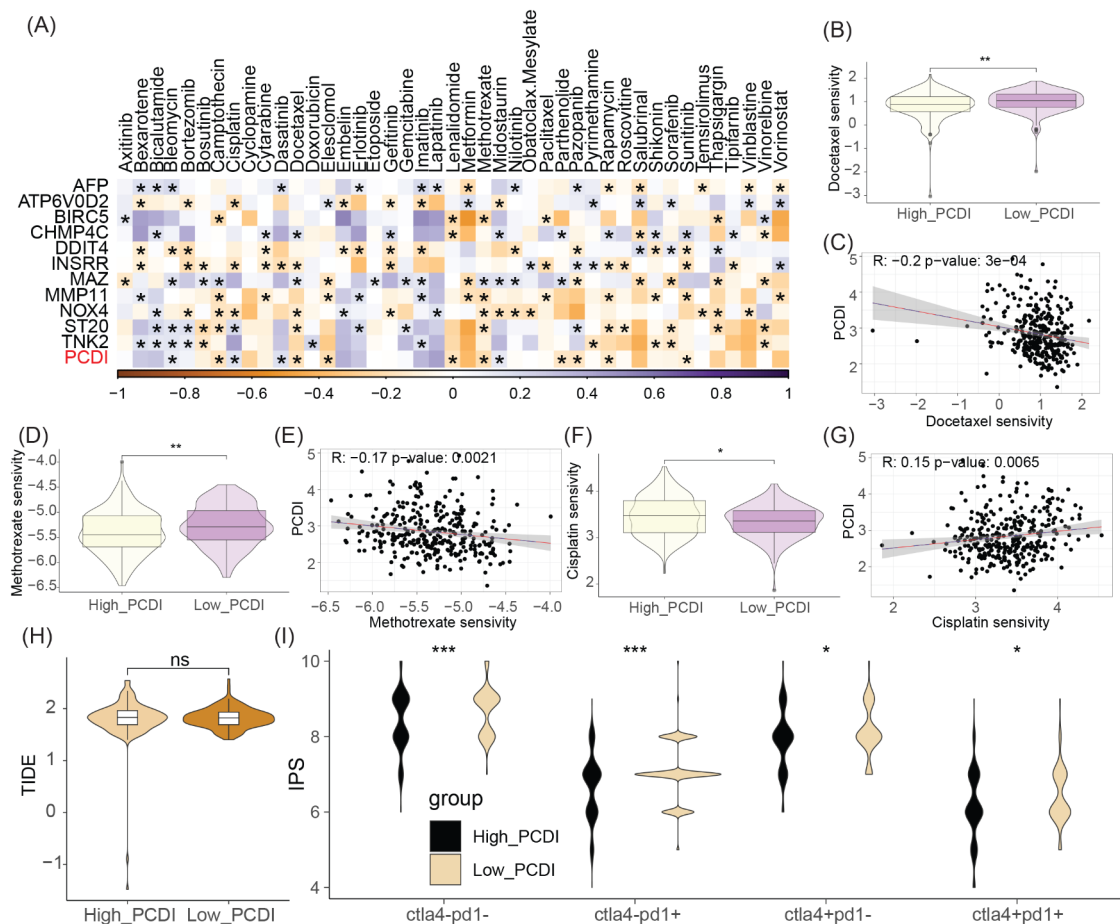


Fig. 7 Dissection of PCDI signature in predicting treatment response. **(A)** Correlation and significance of PCDI expression and drug sensitivity, along with its related PCDRGs. **(B)** Violin plot comparing the sensitivity of Docetaxel between the High_PCDI and Low_PCDI groups. **(C)** Scatter plot showing the correlation between Docetaxel sensitivity and PCDI. **(D)** Violin plot comparing the sensitivity of Methotrexate between the High_PCDI and Low_PCDI groups. **(E)** Scatter plot showing the correlation between Methotrexate sensitivity and PCDI. **(F)** Violin plot comparing the sensitivity of Cisplatin between the High_PCDI and Low_PCDI groups. **(G)** Scatter plot showing the correlation between Cisplatin sensitivity and PCDI. **(H)** Violin plot comparing TIDE scores between the High_PCDI and Low_PCDI groups. **(I)** Violin plot comparing IPS scores between the High_PCDI and Low_PCDI groups. * $p < 0.05$, ** $p < 0.01$, *** $p < 0.001$

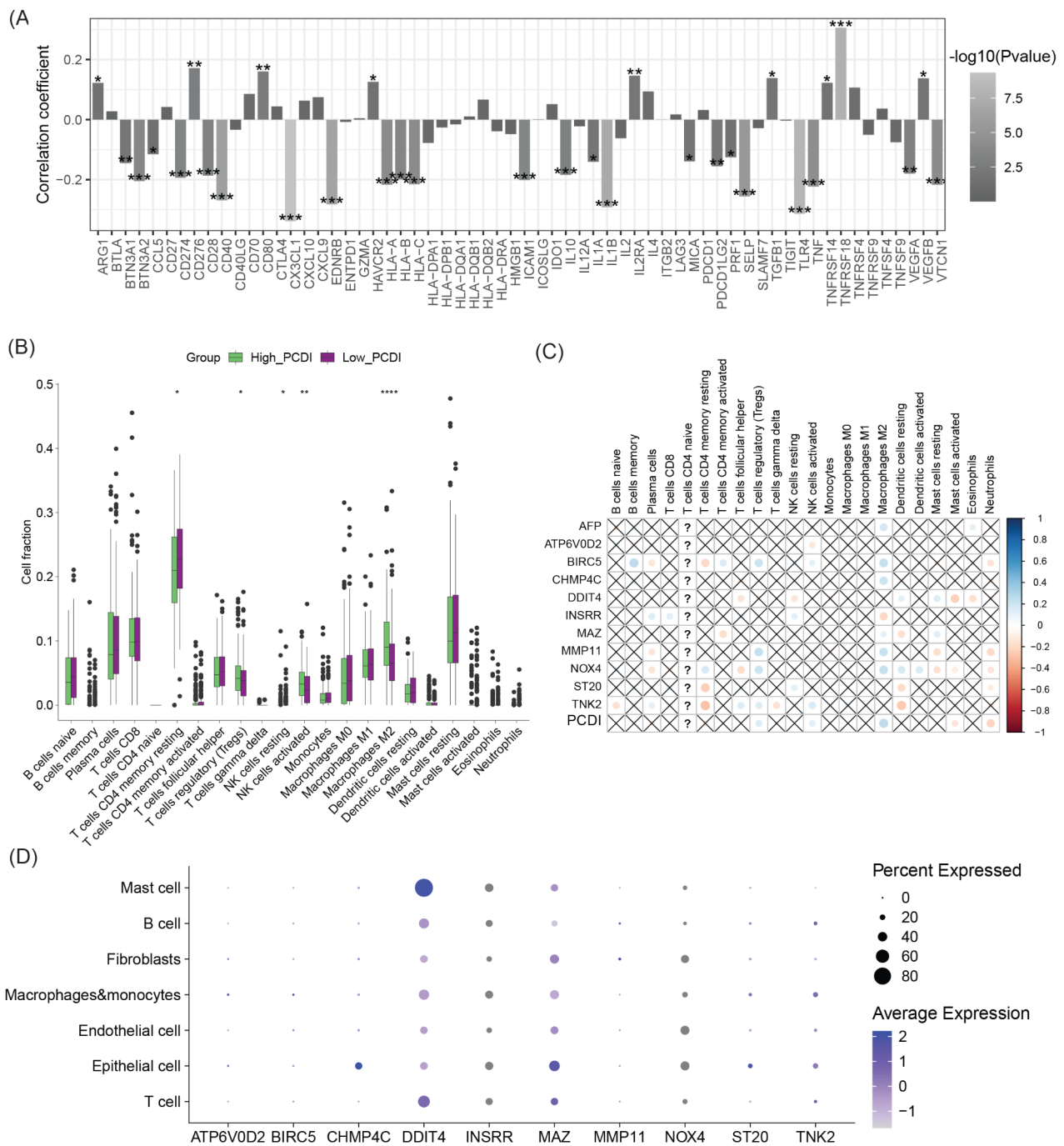


Fig. 8 Dissection of tumor microenvironment based on programmed cell death signature. **(A)** Bar plot showing the correlation between immunomodulators and the PCDI values in PCa patients. **(B)** Boxplots comparing the immune cell infiltration between the High_PCDI and Low_PCDI groups. **(C)** Correlation and significance of PCDI and related PCDRGs with immune cell infiltration. **(D)** Feature plot displaying the expression of PCDI-related PCDRGs in different cell types in the GSE193337 dataset. * $p < 0.05$, ** $p < 0.01$, *** $p < 0.001$, **** $p < 0.0001$

heightened immune activity. Additionally, when comparing the High_PCDI group to the Low_PCDI group, we observed higher levels of M2 macrophage infiltration and reduced levels of T cell and NK cell infiltration (Fig. 8B). Notably, the expression of PCDI and its associated genes exhibited significant correlations with immune

cell infiltration (Fig. 8C). Furthermore, we examined the expression patterns of PCDI-related genes in PCa tissues in comparison to corresponding benign tissues using single-cell RNA transcriptome data. Dot plots demonstrated widespread expression of the majority of PCDI-related genes across various cell types (Fig. 8D), with notable

differential expression between tumor and benign tissues (Figure S2).

Validation of PCDI-related PCDRGs

Immunohistochemical staining images for nine PCDRG proteins associated with the PCDI were collected from the HPA database of prostate cancer and healthy prostate tissue samples. Compared to normal specimens, BIRC5, CHMP4C, MAZ, MMP11, and TNK2 protein

expression levels were elevated in PCa samples, while INSRR and DDIT4 exhibited lower expression levels in line with gene expression data (Fig. 9A). Notably, the differences in protein expression for AFP and ATP6V0D2 were not as pronounced. Consequently, we further assessed the protein expression of AFP, ATP6V0D2, and NOX4 using Western blotting. The results showed that, compared to normal controls, both AFP and NOX4 displayed significantly increased expression in PCa tissues,

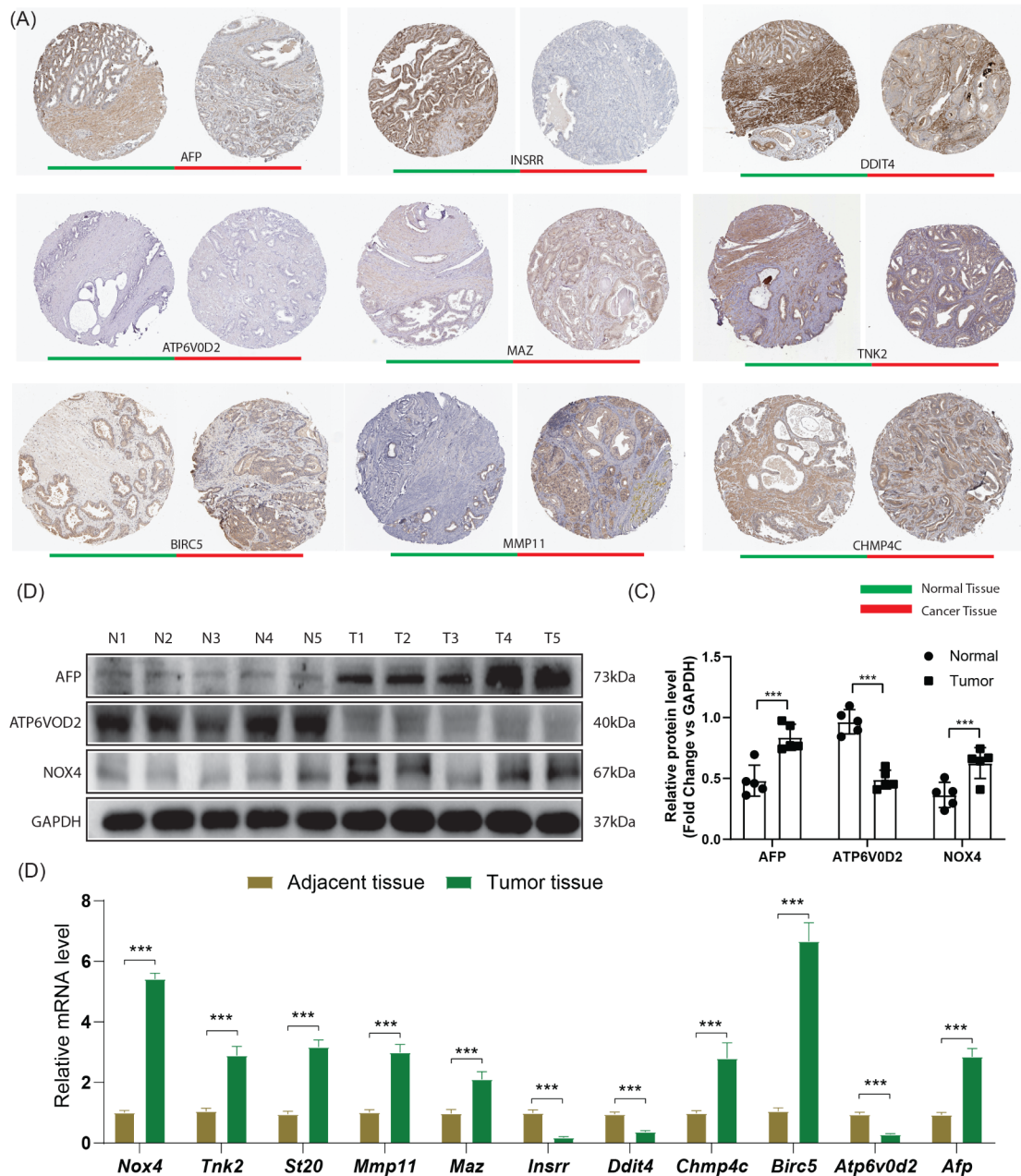


Fig. 9 Validation of PCDRGs in PCDI. **(A)** Protein expression obtained from the human protein atlas (HPA) database in PCa tissues and normal tissues. **(B)** Western blot analysis was employed to assess the protein expression levels of AFP, ATP6V0D2, and NOX4 in cancerous versus adjacent non-cancerous tissues. **(C)** Quantitative analysis of the Western blot data was conducted to determine relative protein expression normalized to GAPDH. **(D)** Gene expression (Fold control) was quantified using quantitative Real-Time Polymerase Chain Reaction (qRT-PCR).

whereas ATP6V0D2 demonstrated a significant decrease in expression (Fig. 9B and C). Furthermore, we quantified the mRNA expression levels of the eleven PCDRGs in PCDI (Fig. 9D). Our findings revealed that eight genes—*Nox4*, *Tnk2*, *St20*, *Mmp11*, *Maz*, *Chmp4c*, *Birc5*, and *Afp*—were significantly overexpressed in prostate cancer (PCa), whereas three genes—*Insrr*, *Ddit4*, and *Atp6v0d2*—exhibited notably reduced expression. These results were in concordance with data from the TCGA-PRAD cohort, thereby further substantiating the potential of these genes as biomarkers for PCa.

Discussion

The biological recurrence of prostate cancer is a complex issue that requires a comprehensive consideration of multiple factors in order to develop personalized treatment strategies. Regular follow-up and examinations are crucial for early detection of biological recurrence and timely adjustment of treatment plans. This study investigates the mechanisms of PCD in malignant tumor progression and systematically examines their predictive capabilities for BCR in patients with prostate cancer. For the first time, 19 distinct patterns of PCD were comprehensively analyzed, elucidating the interplay between prognostic-associated PCD and tumor heterogeneity at the single-cell level in prostate cancer. To evaluate BCR in prostate cancer patients, a PCDI was developed using the TCGA cohort, and its superior performance was subsequently validated in four external cohorts (GSE116918, GSE46602, GSE70769, MSKCC2010). Moreover, the PCDI was integrated with T stage to construct a nomogram that enhances the predictive accuracy and clinical applicability of BCR. Finally, a comprehensive understanding of the relationship between PCDI features, tumor microenvironment, and clinical response was established.

Our analysis unveiled that differentially expressed PCDRGs in PCa are intricately associated with multiple signaling pathways, notably the PI3K-AKT, Ras, and Rap1 pathways. These pathways share a complex interplay with programmed cell death, exerting multifaceted effects on cellular fate determination, either promoting survival or inducing cell demise. The PI3K-AKT signaling cascade, primarily orchestrated by Phosphoinositide 3-kinase (PI3K) and the serine/threonine-specific protein kinase AKT, plays a pivotal role in various cellular processes encompassing growth, proliferation, metabolism, and survival [40]. AKT exerts its anti-apoptotic effects by phosphorylating and inactivating pro-apoptotic proteins such as Bad, Bax, and Forkhead box O (FOXO) transcription factors [41]. Activated Ras can trigger both the MAPK/ERK and PI3K-AKT cascades, both of which inhibit apoptosis and foster cell proliferation [42]. Rap1 is integral to cell adhesion, cytoskeletal rearrangement,

and cell survival. Aberrant activation of the Rap1 signaling pathway can confer resistance to apoptosis, thereby facilitating the survival of tumor cells [43, 44]. Furthermore, our findings illustrated that the PCDI is markedly elevated in older patients as opposed to their younger counterparts, heralding a heightened risk of BCR. With advancing age, the immune system undergoes a series of modifications, collectively referred to as immunosenescence [45]. This includes a diminishment of T and B lymphocyte pools, a decline in immune responsiveness, and the chronic persistence of an inflammatory state. These alterations may impair the body's capability to combat infections and diseases, and simultaneously, they may undermine tumor immune surveillance, potentially amplifying the risk of cancer onset and its subsequent biochemical recurrence.

Programmed cell death encompasses intricate regulatory mechanisms involving various processes. Accumulating evidence suggests that PCD plays a pivotal role in biological processes and has been implicated in the occurrence and metastasis of malignant tumors for decades. In this study, we constructed a feature set comprising 11 PCDRGs (TNK2, ST20, NOX4, MMP11, MAZ, INSR, DDIT4, CHMP4C, BIRC5, ATP6V0D2, AFP) and demonstrated its potential to predict BCR in patients with PCa. The amplification of the TNK2 gene in primary tumors has been associated with poor prognosis, as it facilitates esophageal cancer progression through the EGFR-AKT signaling pathway [46]. NOX4 regulates cancer-associated fibroblast (CAF) differentiation, and its inhibition enhances immune therapy by overcoming CAF-mediated CD8 T cell exclusion [47]. Matrix metalloproteinase 11 (MMP11) participates in extracellular matrix degradation and may exert pro-tumorigenic effects through interactions with cancer cells, monocytes, and endothelial cells [48]. The transcriptional activation of the *kras*-dependent RalGEFs pathway by MAZ promotes prostate cancer bone metastasis, and high MAZ expression is negatively correlated with overall survival and bone metastasis-free survival in PCa patients [49]. Our findings indicate that PCa patients with high MAZ expression are more prone to experience BCR, suggesting the potential of MAZ as a prognostic and therapeutic marker for BCR in PCa patients.

In addition, DDIT4 facilitates cancer cell proliferation and tumorigenesis through the p53 and MAPK pathways and has been identified as an adverse prognostic marker in various malignant tumors, including endometrial cancer and head and neck squamous cell carcinoma [50–52]. However, our analysis revealed that DDIT4 is downregulated in PCa patients and serves as a risk factor for BCR. CHMP4C is upregulated in prostate cancer and associated with poor prognosis, whereas low expression of CHMP4C is linked to better immune response and drug

resistance [53], aligning with the findings of this study. BIRC5, a well-known target for cancer therapy, directly regulates apoptosis and mitosis in cancer cells during tumorigenesis and metastasis. Systematic analysis has demonstrated that BIRC5 overexpression is associated with the occurrence and progression of various cancer types [54], and our study confirms its overexpression in PCa and its positive correlation with BCR. Notably, the copy number of ATP6V0D2 exhibits an inverse correlation with both its gene and protein expression in PCa, suggesting that its transcriptional and translational regulation may involve more intricate mechanisms. Moreover, the role and underlying mechanisms of ATP6V0D2 vary across different malignancies. In esophageal cancer, ATP6V0D2 has been documented as a marker indicative of a poorer prognosis [55], whereas in lung adenocarcinoma, higher expression during the disease's middle stages portends a more favorable outcome [56]. In this study, decreased expression of ATP6V0D2 in PCa patients predicted a lower BCR, potentially linked to increased expression in macrophages. Additionally, ST20 and AFP were upregulated in PCa patients and positively correlated with BCR; however, their specific mechanisms in cancer initiation and progression remain unknown and warrant further investigation.

Enrichment analyses revealed lower enrichment scores for entosis, NETosis, paraptosis, and necroptosis, juxtaposed with a higher enrichment score for ferroptosis within the tumor milieu. These findings underscore the relative significance of distinct modalities of PCD within the tumor microenvironment. Reduced entosis levels may indicate that neoplastic cells have devised alternative survival strategies under these conditions or that the tumor microenvironment is non-conducive to this form of cell demise [26]. The diminution of NETosis in the tumor context might reflect immune evasion tactics employed by tumor cells, such as secretion of factors inhibiting neutrophil activity, or an unsupportive microenvironment for the formation of NETs [57]. Diminished paraptosis may suggest that tumor cells possess enhanced antioxidant defense mechanisms or manage their autophagic processes more efficiently, thereby evading this particular type of cell death [58]. Necroptosis, a programmed necrosis-like cell death pathway mediated by RIPK1 and RIPK3, typically serves as an alternate death route when apoptotic pathways are suppressed. The low enrichment score for necroptosis might denote that tumor cells have developed mechanisms to inhibit this pathway or that the signaling milieu within the tumor microenvironment is not conducive to necroptosis initiation [59]. Ferroptosis, an iron-dependent mode of cell death characterized by lipid peroxidation accumulation, shows a high enrichment score. This could correlate with an increased susceptibility of tumor cells to oxidative stress or may

indicate that the redox state within the tumor microenvironment facilitates this type of cell death [60]. Some tumor cells may resist chemotherapeutic agents through mechanisms that suppress ferroptosis, whereas others may be more susceptible due to deficiencies in antioxidants or dysregulation of iron metabolism [61].

In the realm of cancer treatment, chemotherapy and immunotherapy have been identified as potential strategies in combating cancer cells by promoting PCD. The present explored the interplay between the PCDI and drug sensitivity as well as the response to immune therapy. Notably, PCDI exhibited a negative correlation with drug sensitivity across various drugs, while PCa patients displaying lower PCDI levels exhibited a heightened response to immune therapy, thus suggesting a potential benefit from immunotherapy. Multiple genes comprising the PCDI have been substantiated to influence drug sensitivity and immunotherapy efficacy. For instance, NOX4 regulates chemoresistance and immune therapy responsiveness through modulation of IL-8, PD-L1, and TNF- α [62, 63]. MMP11, a constituent of the MMP family, has been shown to regulate cisplatin resistance in advanced gastric adenocarcinoma upon upregulation [64]. Additionally, genes such as MAZ [65], DDIT4 [66], and BIRC5 [67] have been validated for their associations with drug sensitivity. Collectively, the synergistic action of these genes establishes the correlation between the PCDI, drug sensitivity, and immunotherapy responsiveness. These compelling findings shed light on the potential utilization of PCDI as a personalized treatment planning tool for PCa patients.

The tumor microenvironment has been acknowledged to play a pivotal role in the realm of drug sensitivity and immune therapy response. For example, the tumor microenvironment possesses the capacity to influence the delivery of drugs to tumor cells, thereby impacting the efficacy of drug treatments. Immune cells and fibroblasts within the tumor microenvironment can secrete factors that instigate drug resistance in tumor cells [68]. Additionally, the interaction between immune cells and tumor cells within the tumor microenvironment can exert an influence on the effectiveness of immune therapy [69]. Intriguingly, low levels of PCDI in PCa patients have been associated with an increased infiltration of T cells and NK cells, alongside a diminished infiltration of M2 macrophages. Moreover, the correlation between PCDI and the expression of immune regulatory markers suggests a potential mapping relationship between PCDI and the tumor immune microenvironment. These significant associations lay the groundwork for establishing a correlation between PCDI and both drug sensitivity and immune therapy response. Further experimental exploration is warranted to elucidate the underlying mechanisms

behind PCDI-related gene prediction of treatment response in PCa patients.

Notwithstanding the commendable performance exhibited by the model in both the training and validation cohorts, it is imperative to acknowledge certain limitations that necessitate attention. Primarily, the utilization of retrospective analysis relying on public databases may impart a degree of bias, thereby underscoring the need for additional prospective studies to substantiate the validity of the model. Furthermore, our model has yet to comprehensively investigate the biological functions of specific PCDRGs (ST20 and AFP) in malignant tumors, thereby warranting further experimental research to unravel the functional significance of PCDI and fortify the reliability of our findings.

Conclusion

In summary, the present study systematically elucidated the prognostic, tumor heterogeneity, and treatment response characteristics associated with 19 PCD patterns in PCa patients. Through the incorporation of 11 PCDRGs, a robust PCa patient prediction model for BCR was developed. Moreover, a clinically applicable nomogram, which integrated T stage, was constructed, thereby presenting a valuable tool for accurate prognosis assessment in PCa patients.

Supplementary Information

The online version contains supplementary material available at <https://doi.org/10.1186/s12935-024-03462-7>.

Supplementary Material 1

Supplementary Material 2

Supplementary Material 3

Acknowledgements

Not applicable.

Author contributions

All of the authors have read and approved the final manuscript. Ming Wang and Bangshun Dai conceived and designed the research; Qiushi Liu and Bangshun Dai were responsible for data analysis. All authors contributed to manuscript writing and revisions.

Funding

Not applicable.

Data availability

Data used to support the findings of this study are available from the corresponding author upon request.

Declarations

Ethics approval and consent to participate

Not applicable.

Consent for publication

Not applicable.

Competing interests

The authors declare no competing interests.

Author details

¹Department of Urology, First Affiliated Hospital of Anhui Medical University, Anhui Medical University, No. 218 Jixi Road, Hefei, Anhui, China

Received: 5 February 2024 / Accepted: 28 July 2024

Published online: 24 August 2024

References

- Jemal A, Ma J, Siegel R, Fedewa S, Brawley O, Ward EM. Prostate Cancer Incidence Rates 2 years after the US Preventive Services Task Force Recommendations against Screening. *Jama Oncol*. 2016;2(12):1657–60.
- Bergengren O, Pekala KR, Matsoukas K, Fainberg J, Mungovan SF, Bratt O, et al. 2022 update on prostate Cancer epidemiology and risk Factors-A systematic review. *Eur Urol*. 2023;84(2):191–206.
- Pernar CH, Ebot EM, Wilson KM, Mucci LA. The epidemiology of prostate Cancer. *Cold Spring Harb Perspect Med*. 2018;8(12).
- Hao Y, Bjerke GA, Pietrzak K, Melhuish TA, Han Y, Turner SD, et al. TGF β signaling limits lineage plasticity in prostate cancer. *Plos Genet*. 2018;14(5):e1007409.
- Small EJ, Saad F, Chowdhury S, Oudard S, Hadaschik BA, Graff JN, et al. Apalutamide and overall survival in non-metastatic castration-resistant prostate cancer. *Ann Oncol*. 2019;30(11):1813–20.
- Simon NI, Parker C, Hope TA, Paller CJ. Best approaches and updates for prostate Cancer biochemical recurrence. *Am Soc Clin Oncol Educ Book*. 2022;42:1–8.
- Galluzzi L, Vitale I, Aaronson SA, Abrams JM, Adam D, Agostinis P, et al. Molecular mechanisms of cell death: recommendations of the nomenclature Committee on Cell Death 2018. *Cell Death Differ*. 2018;25(3):486–541.
- Liu X, Zhuang L, Gan B. Disulfidoptosis: disulfide stress-induced cell death. *Trends Cell Biol*. 2023.
- Green DR. The death receptor pathway of apoptosis. *Cold Spring Harb Perspect Biol*. 2022;14(2).
- Yu P, Zhang X, Liu N, Tang L, Peng C, Chen X. Pyroptosis: mechanisms and diseases. *Signal Transduct Target Ther*. 2021;6(1):128.
- Jiang X, Stockwell BR, Conrad M. Ferroptosis: mechanisms, biology and role in disease. *Nat Rev Mol Cell Biol*. 2021;22(4):266–82.
- Debnath J, Gammoh N, Ryan KM. Autophagy and autophagy-related pathways in cancer. *Nat Rev Mol Cell Biol*. 2023;24(8):560–75.
- Yan J, Wan P, Choksi S, Liu ZG. Necroptosis and tumor progression. *Trends Cancer*. 2022;8(1):21–7.
- Xie J, Yang Y, Gao Y, He J. Cuproptosis: mechanisms and links with cancers. *Mol Cancer*. 2023;22(1):46.
- Zhou Y, Liu L, Tao S, Yao Y, Wang Y, Wei Q, et al. Parthanatos and its associated components: promising therapeutic targets for cancer. *Pharmacol Res*. 2021;163:105299.
- Hamann JC, Kim SE, Overholtzer M. Methods for the study of Entotic Cell Death. *Methods Mol Biol*. 2019;1880:447–54.
- Inoue M, Enomoto M, Yoshimura M, Mizowaki T. Pharmacological inhibition of sodium-calcium exchange activates NADPH oxidase and induces infection-independent NETotic cell death. *Redox Biol*. 2021;43:101983.
- Nakamura H, Tanaka T, Zheng C, Afione SA, Warner BM, Noguchi M, et al. Lysosome-Associated Membrane Protein 3 induces lysosome-dependent cell death by impairing autophagic caspase 8 degradation in the salivary glands of individuals with Sjögren's Disease. *Arthritis Rheumatol*. 2023;75(9):1586–98.
- Chen F, Kang R, Liu J, Tang D. Mechanisms of alkaliptosis. *Front Cell Dev Biol*. 2023;11:1213995.
- Holze C, Michaudel C, Mackowiak C, Haas DA, Benda C, Hubel P, et al. Oxeiptosis, a ROS-induced caspase-independent apoptosis-like cell-death pathway. *Nat Immunol*. 2018;19(2):130–40.
- Thiam HR, Wong SL, Wagner DD, Waterman CM. Cellular mechanisms of NETosis. *Annu Rev Cell Dev Biol*. 2020;36:191–218.
- Kroemer G, Galluzzi L, Kepp O, Zitvogel L. Immunogenic cell death in cancer therapy. *Annu Rev Immunol*. 2013;31:51–72.
- Taddei ML, Giannoni E, Fiaschi T, Chiarugi P. Anoikis: an emerging hallmark in health and diseases. *J Pathol*. 2012;226(2):380–93.
- Hanson S, Dharan A, P VJ, Pal S, Nair BG, Kar R, et al. Paraptosis: a unique cell death mode for targeting cancer. *Front Pharmacol*. 2023;14:1159409.

25. Bielsa N, Casasampere M, Abad JL, Enrich C, Delgado A, Fabriàs G et al. Methuosis contributes to Jaspine-B-Induced cell death. *Int J Mol Sci*. 2022;23(13).
26. Mlynarczuk-Bialy I, Dziuba I, Sarnecka A, Platos E, Kowalczyk M, Pels KK et al. Entosis: from Cell Biology to Clinical Cancer Pathology. *Cancers (Basel)*. 2020;12(9).
27. Zheng P, Zhou C, Ding Y, Duan S. Disulfidptosis: a new target for metabolic cancer therapy. *J Exp Clin Cancer Res*. 2023;42(1):103.
28. Qin H, Abulaiti A, Maimaiti A, Abulaiti Z, Fan G, Aili Y, et al. Integrated machine learning survival framework develops a prognostic model based on inter-crosstalk definition of mitochondrial function and cell death patterns in a large multicenter cohort for lower-grade glioma. *J Transl Med*. 2023;21(1):588.
29. Zheng T, Liu Q, Xing F, Zeng C, Wang W. Disulfidptosis: a new form of programmed cell death. *J Exp Clin Cancer Res*. 2023;42(1):137.
30. Song K, Li L, Zhang G. Bias and correction in RNA-seq data for Marine species. *Mar Biotechnol (Ny)*. 2017;19(5):541–50.
31. Leek JT, Johnson WE, Parker HS, Jaffe AE, Storey JD. The sva package for removing batch effects and other unwanted variation in high-throughput experiments. *Bioinformatics*. 2012;28(6):882–3.
32. Mayakonda A, Lin DC, Assenov Y, Plass C, Koeffler HP. Maftools: efficient and comprehensive analysis of somatic variants in cancer. *Genome Res*. 2018;28(11):1747–56.
33. Zhang H, Meltzer P, Davis S. RCircos: an R package for Circos 2D track plots. *BMC Bioinformatics*. 2013;14:244.
34. Yu G, Wang LG, Han Y, He QY. clusterProfiler: an R package for comparing biological themes among gene clusters. *Omics*. 2012;16(5):284–7.
35. Gentles AJ, Newman AM, Liu CL, Bratman SV, Feng W, Kim D, et al. The prognostic landscape of genes and infiltrating immune cells across human cancers. *Nat Med*. 2015;21(8):938–45.
36. Geeleher P, Cox N, Huang RS. pRRophetic: an R package for prediction of clinical chemotherapeutic response from tumor gene expression levels. *PLoS ONE*. 2014;9(9):e107468.
37. Charoentong P, Finotello F, Angelova M, Mayer C, Efremova M, Rieder D, et al. Pan-cancer immunogenomic analyses reveal genotype-immunophenotype relationships and predictors of response to checkpoint blockade. *Cell Rep*. 2017;18(1):248–62.
38. Jiang P, Gu S, Pan D, Fu J, Sahu A, Hu X, et al. Signatures of T cell dysfunction and exclusion predict cancer immunotherapy response. *Nat Med*. 2018;24(10):1550–8.
39. Heidegger I, Fotakis G, Offermann A, Goveia J, Daum S, Salcher S, et al. Comprehensive characterization of the prostate tumor microenvironment identifies CXCR4/CXCL12 crosstalk as a novel antiangiogenic therapeutic target in prostate cancer. *Mol Cancer*. 2022;21(1):132.
40. Yu JS, Cui W. Proliferation, survival and metabolism: the role of PI3K/AKT/mTOR signalling in pluripotency and cell fate determination. *Development*. 2016;143(17):3050–60.
41. Brunet A, Bonni A, Zigmond MJ, Lin MZ, Juo P, Hu LS, et al. Akt promotes cell survival by phosphorylating and inhibiting a forkhead transcription factor. *Cell*. 1999;96(6):857–68.
42. Mendoza MC, Er EE, Blenis J. The Ras-ERK and PI3K-mTOR pathways: cross-talk and compensation. *Trends Biochem Sci*. 2011;36(6):320–8.
43. Chen B, Chen L, Yang J, Hou M, Cai Q, Dai W, et al. Cepharanthine inhibits migration, invasion, and EMT of bladder cancer cells by activating the Rap1 signaling pathway in vitro. *Am J Transl Res*. 2024;16(5):1602–19.
44. Li X, Qian H, Ye H, Zhao H, Cui J, Fang X, et al. DEHP induces apoptosis and autophagy of the thyroid via Rap1 signaling pathway: in vivo and in vitro study. *Food Chem Toxicol*. 2024;187:114609.
45. Nikolich-Zugich J. The twilight of immunity: emerging concepts in aging of the immune system. *Nat Immunol*. 2018;19(1):10–9.
46. Zhang A, Zhang R, Yang Z, Tian R. TNK2 promoted esophageal cancer progression via activating egfr-akt signaling. *J Clin Lab Anal*. 2021;35(3):e23700.
47. Ford K, Hanley CJ, Mellone M, Szyndralewicz C, Heitz F, Wiesel P, et al. NOX4 inhibition potentiates immunotherapy by overcoming Cancer-Associated fibroblast-mediated CD8 T-cell exclusion from tumors. *Cancer Res*. 2020;80(9):1846–60.
48. Kang SU, Cho SY, Jeong H, Han J, Chae HY, Yang H, et al. Matrix metalloproteinase 11 (MMP11) in macrophages promotes the migration of HER2-positive breast cancer cells and monocyte recruitment through CCL2-CCR2 signaling. *Lab Invest*. 2022;102(4):376–90.
49. Yang Q, Lang C, Wu Z, Dai Y, He S, Guo W, et al. MAZ promotes prostate cancer bone metastasis through transcriptionally activating the KRas-dependent RalGEFs pathway. *J Exp Clin Cancer Res*. 2019;38(1):391.
50. Du F, Sun L, Chu Y, Li T, Lei C, Wang X, et al. DDIT4 promotes gastric cancer proliferation and tumorigenesis through the p53 and MAPK pathways. *Cancer Commun (Lond)*. 2018;38(1):45.
51. Yoshikawa N, Yoshida K, Liu W, Matsukawa T, Hattori S, Yoshihara M, et al. The prognostic significance of DDIT4 in endometrial cancer. *Cancer Biomark*. 2023;37(4):217–25.
52. Zhang Z, Zhu H, Zhao C, Liu D, Luo J, Ying Y, et al. DDIT4 promotes malignancy of head and neck squamous cell carcinoma. *Mol Carcinog*. 2023;62(3):332–47.
53. Zhang H, Liu D, Qin Z, Yi B, Zhu L, Xu S, et al. CHMP4C as a novel marker regulates prostate cancer progression through cycle pathways and contributes to immunotherapy. *Front Oncol*. 2023;13:1170397.
54. Fäldt BA, Larsson P, Helou K, Einbeigi Z, Parris TZ. Pan-cancer analysis identifies BIRC5 as a prognostic biomarker. *BMC Cancer*. 2022;22(1):322.
55. Qi M, Liu DM, Ji W, Wang HL. ATP6V0D2, a subunit associated with proton transport, serves an oncogenic role in esophagus cancer and is correlated with epithelial-mesenchymal transition. *Esophagus*. 2020;17(4):456–67.
56. Liu N, Luo J, Kuang D, Xu S, Duan Y, Xia Y, et al. Lactate inhibits ATP6V0d2 expression in tumor-associated macrophages to promote HIF-2 α -mediated tumor progression. *J Clin Invest*. 2019;129(2):631–46.
57. Demkow U. Neutrophil Extracellular traps (NETs) in Cancer Invasion, Evasion and Metastasis. *Cancers (Basel)*. 2021;13(17).
58. Xu CC, Lin YF, Huang MY, Zhang XL, Wang P, Huang MQ, et al. Paraptosis: a non-classical paradigm of cell death for cancer therapy. *Acta Pharmacol Sin*. 2024;45(2):223–37.
59. Seo J, Nam YW, Kim S, Oh DB, Song J. Necroptosis molecular mechanisms: recent findings regarding novel necroptosis regulators. *Exp Mol Med*. 2021;53(6):1007–17.
60. Jin X, Tang J, Qiu X, Nie X, Ou S, Wu G, et al. Ferroptosis: emerging mechanisms, biological function, and therapeutic potential in cancer and inflammation. *Cell Death Discov*. 2024;10(1):45.
61. Wang Y, Han J, Zhan S, Guo C, Yin S, Zhan L, et al. Fucoidan alleviates doxorubicin-induced cardiotoxicity by inhibiting ferroptosis via Nrf2/GPX4 pathway. *Int J Biol Macromol*. 2024;276(Pt 1):133792.
62. Liu WJ, Wang L, Zhou FM, Liu SW, Wang W, Zhao EJ, et al. Elevated NOX4 promotes tumorigenesis and acquired EGFR-TKIs resistance via enhancing IL-8/PD-L1 signaling in NSCLC. *Drug Resist Updat*. 2023;70:100987.
63. Wang LJ, Chiou JT, Lee YC, Chang LS. Docetaxel-triggered S1D2/NOX4/JNK/HuR signaling axis is associated with TNF- α -mediated apoptosis of cancer cells. *Biochem Pharmacol*. 2022;195:114865.
64. Liu S, Wu M, Peng M. Circ_0000260 regulates the development and deterioration of gastric adenocarcinoma with Cisplatin Resistance by Upregulating MMP11 via Targeting MiR-129-5p. *Cancer Manag Res*. 2020;12:10505–19.
65. Wang T, Zhu X, Wang K, Li J, Hu X, Lin P, et al. Transcriptional factor MAZ promotes cisplatin-induced DNA damage repair in lung adenocarcinoma by regulating NEIL3. *Pulm Pharmacol Ther*. 2023;80:102217.
66. Chen X, Li Z, Liang M, Zhang Z, Zhu D, Lin B, et al. Identification of DDIT4 as a potential prognostic marker associated with chemotherapeutic and immunotherapeutic response in triple-negative breast cancer. *World J Surg Oncol*. 2023;21(1):194.
67. Fan Y, Pan Y, Jia L, Gu S, Liu B, Mei Z et al. BIRC5 facilitates cisplatin-chemoresistance in a m(6) A-dependent manner in ovarian cancer. *Cancer Med*. 2023;13(1).
68. Zhang A, Miao K, Sun H, Deng CX. Tumor heterogeneity reshapes the tumor microenvironment to influence drug resistance. *Int J Biol Sci*. 2022;18(7):3019–33.
69. Pitt JM, Marabelle A, Eggermont A, Soria JC, Kroemer G, Zitvogel L. Targeting the tumor microenvironment: removing obstruction to anticancer immune responses and immunotherapy. *Ann Oncol*. 2016;27(8):1482–92.

Publisher's Note

Springer Nature remains neutral with regard to jurisdictional claims in published maps and institutional affiliations.